Supporting Information: Limits to the Optical Response of Graphene and 2D Materials

Owen D. Miller,[*,†] Ognjen Ilic,[‡] Thomas Christensen,[¶] M. T. Homer Reid,[§] Harry A. Atwater,[‡] John D. Joannopoulos,[¶] Marin Soljačić,[¶] and Steven G. Johnson[¶]

†*Department of Applied Physics, Yale University, New Haven, CT 06511*

‡*Department of Applied Physics and Material Science, California Institute of Technology, Pasadena, CA 91125*

¶*Department of Physics, Massachusetts Institute of Technology, Cambridge, MA 02139*

§*Department of Mathematics, Massachusetts Institute of Technology, Cambridge, MA 02139*

E-mail: owen.miller@yale.edu

Contents

1 Optimized structure to reach within 1% of extinction bound

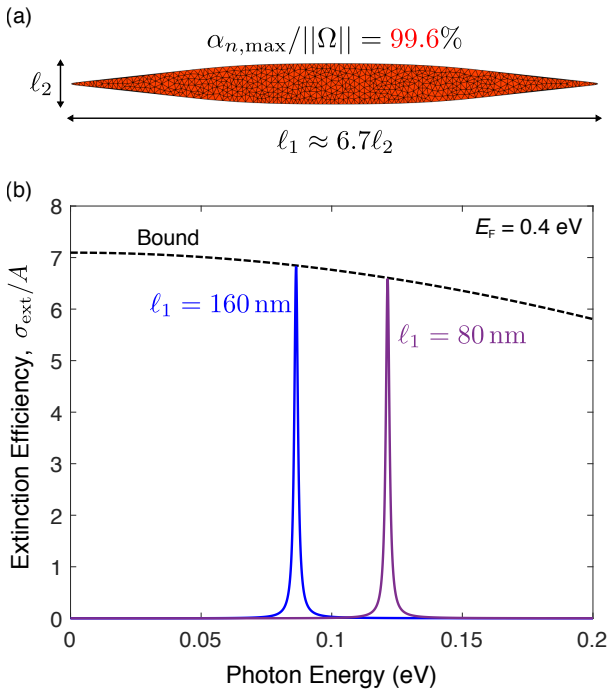

Figure S1: (a) "Pinched ellipse" geometry, described by Eq. (1), with the parameters in Eq. (2). The pinched ellipse geometry has a mode with 99.6% of the maximum polarizability possible, such that the response is almost perfectly concentrated at a single resonant frequency. (b) Spectral response of the pinched-ellipse geometry, for two different scaling factors (given by the widths of the structures). The response achieves 99.6% of the general bound.

In this section we show that the bounds can be reached to within 1% through simple optimization of the scattering structure. The elliptical disks considered in the main text only have two degrees of freedom, one of which is a scaling parameter that solely shifts the

frequency. Thus, we consider the "pinched ellipse" structure depicted in Fig. S1. Utilizing the angle θ in the two-dimensional plane of the structure, the boundary of a simple ellipse can be parameterized as $x = a\cos\theta$, $y = \sin\theta$. We generate the pinched ellipse via the parameterization:

$$x = a\cos\theta \tag{1a}$$

$$y = \sin\theta\left[1 + de^{-|x(\theta)|^s/w}\right] \tag{1b}$$

where a, d, s, and w are free parameters. Many different combinations can lead to good performance; from simple unconstrained optimizations, the values

$$a = 53.788 \tag{2a}$$

$$d = 3.0917 \tag{2b}$$

$$s = 3.6358 \tag{2c}$$

$$w = 0.3964 \tag{2d}$$

reach near-ideal performance. The performance of such a structure is exhibited not only in the peak of the spectral response but also in the quasistatic polarizability. The quasistatic polarizability of a 2D scatterer, $\alpha(\omega)$, can be decomposed into a complete set of modes that are orthonormal under a properly chosen inner product. The polarizabilities of the modes, α_n for mode n, must satisfy the sum rule[1]

$$\sum_n \alpha_n \leq ||\Omega|| \tag{3}$$

where $||\Omega||$ is the total surface area of the scatterer.

The capability of a structure to reach the bounds developed in the main text is directly related to whether its response is concentrated into a single mode at the frequency of interest. The elliptical disks of the main text have oscillator strengths, i.e., mode polarizabilities, of

approximately 90%, explaining their large extinction cross-sections that reach within 10% of the bounds. For the pinched ellipse of Fig. S1, the parameter values in Eq. (2) yield a normalized oscillator strength of 99.6%, as computed by a quasistatic integral-equation solver[2] and shown in Fig. S1(a). Such a large oscillation strength indicates that the scatterer should reach 99.6% of the extinction bound, which we verify numerically. The nearly ideal spectral response is shown in Fig. S1(b), for two scaled versions of the ellipse shown in Fig. S1(a) with the parameters given in Eq. (2).

2 Optimal conductive heat transfer through graphene

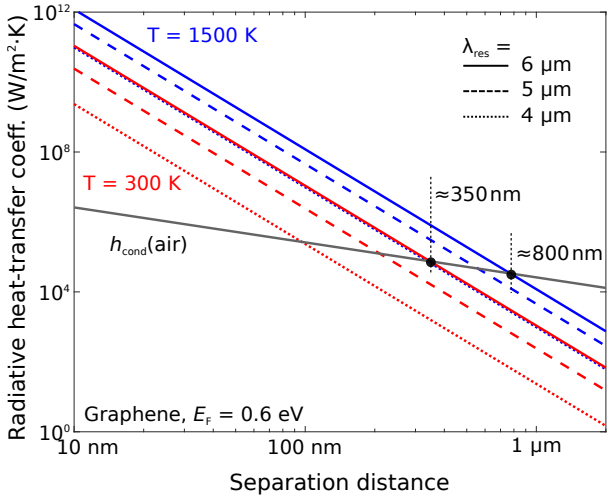

Figure S2: Optimal radiative heat-transfer coefficient for near-field energy exchange between graphene structures operating at the maximum theoretical flux rate, over a bandwidth dictated by the material loss rate. At 300 K it is possible for graphene RHT to surpass conductive transfer through air at ≈ 350 nm separation distance; at 1500 K, it is possible at almost 800 nm separations. The theoretical RHT coefficient increases with the resonant wavelength, λ_{res}, due to the increasing material FOM $|\sigma|^2/\operatorname{Re}\sigma$ of graphene with increasing wavelength.

We showed in Eq. (8) of the main text that near-field radiative heat transfer (RHT) has a unique $1/d^4$ separation-distance dependence for 2D materials, increasing more rapidly than the $1/d^3$ dependence of 3D materials. Here we consider the potential for a 2D material such as graphene to exhibit large radiative heat transfer relative to the large *conductive* heat transfer rate for two bodies separated by micron-scale air gaps. As discussed

in the main text, the total radiative heat transfer between two bodies is given by $H = \int \Phi(\omega) \left[\Theta(\omega, T_1) - \Theta(\omega, T_2)\right] \mathrm{d}\omega$. For a small temperature differential between the bodies, the *conductance* (heat transfer per unit temperature) per area A is termed the *radiative heat transfer coefficient* and is given by

$$h_{\mathrm{rad}} = \frac{1}{A} \int \Phi(\omega) \frac{\partial \Theta}{\partial T} \, \mathrm{d}\omega = \frac{1}{A} k_B \int \Phi(\omega) f(\omega) \, \mathrm{d}\omega, \tag{4}$$

where

$$f(\omega) = \left(\frac{\hbar\omega}{k_B T}\right)^2 \frac{e^{\hbar\omega/k_B T}}{\left(e^{\hbar\omega/k_B T} - 1\right)^2} \tag{5}$$

For common 2D materials such as graphene, the material loss rates are sufficiently small that resonant response is sharply peaked, with a width determined by the material loss. For resonant response the distribution of $\Phi(\omega)$ will be much sharper than the Boltmann-like distribution $f(\omega)$ in the integrand. Thus we can approximate h by

$$h_{\mathrm{rad}} \approx \frac{1}{A} k_B f(\omega_{\mathrm{res}}) \int \Phi(\omega) \, \mathrm{d}\omega \tag{6}$$

$$\approx \frac{1}{A} k_B f(\omega_{\mathrm{res}}) \Phi(\omega_{\mathrm{res}}) \frac{\pi \Delta\omega}{2} \tag{7}$$

where ω_{res} is the peak resonant frequency, and the second approximation assumed a Lorentzian distribution for Φ, with $\Delta\omega$ as the full-width at half-maximum of the distribution. For a plasmonic material such as graphene, we can model the bandwidth through the quality factor: $Q = \frac{\omega}{\Delta\omega} = \frac{|\operatorname{Im}\sigma|}{\operatorname{Re}\sigma}$, which is the 2D-material version of the well-known expression $Q = |\operatorname{Re}\chi| / \operatorname{Im}\chi$ (Refs.[3,4]). For graphene and similar materials at optical frequencies, $\operatorname{Im}\sigma \approx |\sigma|$. Thus if we use the minimal material-dependent bandwidth $\Delta\omega \approx \omega_{\mathrm{res}} \operatorname{Re}\sigma / |\sigma|$, and insert the bound for Φ/A from Eq. (8) in the main text into Eq. (7), we find a bound

on the radiative heat-transfer coefficient:

$$h_{\mathrm{rad}} \leq \frac{3}{16\pi^2}\frac{k_B\omega_{\mathrm{res}}}{d^2}f(\omega_{\mathrm{res}})\frac{|\sigma|^3 Z_0^2}{\mathrm{Im}\,\sigma}\frac{1}{k_{\mathrm{res}}^2 d^2}. \tag{8}$$

Note that this is not a strict bound, but rather an indication of what is *possible*, if the single-frequency bounds derived in the text can be reached over a typical plasmonic bandwidth (which is significantly narrower than the RHT flux rates seen in Fig. 4 of the main text).

Figure S2 shows the heat-transfer coefficient in graphene if Eq. (8) can be met. We fix the Fermi level at 0.6 eV, consider two temperatures: $T = 300\,\mathrm{K}$ and $T = 1500\,\mathrm{K}$, for a resonant wavelength λ_{res} swept from $3\,\mu$m to $5\,\mu$m. For the sake of comparison, we include the *conductive* heat-transfer coefficient through air, taking the thermal conductivity to be $\kappa_{\mathrm{air}} = 0.026\,\mathrm{W/m^2\cdot K}$ (Ref. 5). An exciting feature of Fig. S2 is the length scale at which heat transfer may become dominated by radiative rather than conductive heat transfer. For 300 K, this transition can occur at separation distances larger than 300 nm, and for 1500 K, the transition can happen beyond 800 nm, separations orders of magnitude larger than those required with conventional designs.

3 Graphene material figure of merit: second-order approximation

A surprise in the material figure of merit of graphene is the extent to which interband contributions play a significant role in the peak magnitude of the response even at energies smaller than the Fermi level. The simplified expressions for graphene's material FOM given in Eq. (9) of the main text are asymptotic expressions, and the low-energy expression is only valid for $\omega \ll \gamma$, where γ is the small material loss rate. In this section, we derive a higher-order correction that more accurately describes a broader frequency range. For $\hbar\omega < 2E_{\mathrm{F}}$, the low-temperature ($T \ll E_{\mathrm{F}}/k_B$) approximations of the intra- and interband

conductivities are

$$\sigma_{\text{intra}} = \frac{ie^2}{4\pi\hbar}\frac{4E_{\text{F}}}{\hbar(\omega+i\gamma)} \tag{9a}$$

$$\sigma_{\text{inter}} = -\frac{ie^2}{4\pi\hbar}\ln\left(\frac{2E_{\text{F}}+\hbar(\omega+i\gamma)}{2E_{\text{F}}-\hbar\left(\omega+i\gamma\right)}\right). \tag{9b}$$

A Taylor expansion in frequency (with small parameter $\hbar(\omega+i\gamma)/2E_{\text{F}}$) yields an inverse total conductivity of

$$(Z_0\sigma)^{-1} \simeq -\frac{i}{\alpha}\frac{\hbar(\omega+i\gamma)}{4E_{\text{F}}}\left(1+\frac{\hbar^2(\omega^2-\gamma^2+2i\gamma\omega)}{4E_{\text{F}}^2}\right). \tag{10}$$

Inserting the inverse conductivity of Eq. (10) into the cross-section bound, Eq. (6) of the main text, yields the approximate graphene bound:

$$\begin{aligned}\left(\frac{\sigma_{\text{ext}}}{A}\right)_{\text{bound}} &= \left[\text{Re}\left(Z_0\sigma\right)^{-1}\right]^{-1} \\ &\simeq 4\alpha\left(\frac{E_{\text{F}}}{\hbar\gamma}\right)-\alpha\frac{\hbar\gamma}{E_{\text{F}}}\left[3\left(\frac{\omega}{\gamma}\right)^2-1\right]\end{aligned} \tag{11}$$

Equation (11) predicts a quadratic reduction in graphene's material figure of merit (and thus its response bounds) as a function of energy. As shown in Fig. S2, the quadratic dependence is a good approximation of the full local-response material conductivity for energies well below twice the Fermi level. Note that the frequency-dependent second term in Eq. (11) arises entirely from *inter*band contributions to the conductivity, which are a crucial limiting factors even at frequencies well below the Fermi level.

4 Variational-calculus derivation of upper bounds

Here we provide the intermediate mathematical steps in the derivation of the bounds that appear in Eqs. (4–8) of the main text. For generality, we also accommodate the possibility of magnetic surface currents in addition to electric surface currents. We denote the fields as

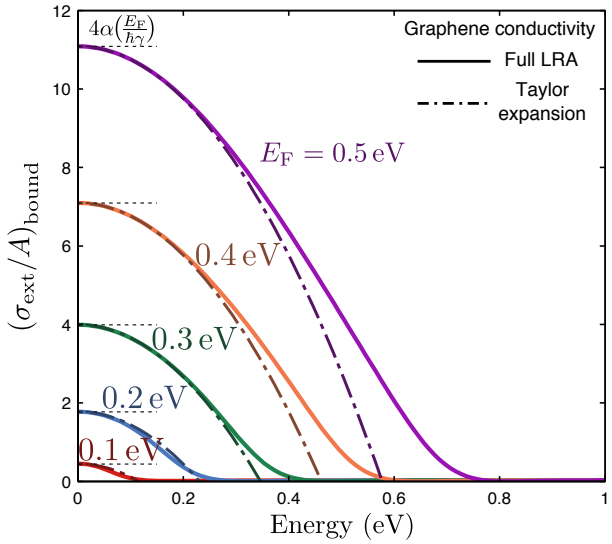

Figure S3: Comparison of the extinction bounds, $(\sigma_{\mathrm{ext}}/A)_{\mathrm{bound}}$, for graphene with the full local-response-approximation (LRA) conductivity (solid) and with the second-order approximation in Eq. (11) (dash-dot). Even at frequencies below the Fermi level, inclusion of the interband terms, resulting in the quadratic dependence evident here, yields much better agreement than the intraband-only expression (dashed).

components of a six-vector ψ,

$$\psi = \begin{pmatrix} \mathbf{E} \\ \mathbf{H} \end{pmatrix} \tag{12}$$

and the electric ($\mathbf{K}$) and magnetic ($\mathbf{N}$) surface currents as components of a six-vector ϕ:

$$\phi = \begin{pmatrix} \mathbf{K} \\ \mathbf{N} \end{pmatrix} \tag{13}$$

Then we can write the absorption and extinction as the inner products of the fields and currents:

$$P_{\mathrm{abs}} = \frac{1}{2}\,\mathrm{Re}\,\langle \psi, \phi \rangle \tag{14}$$

$$P_{\mathrm{ext}} = \frac{1}{2}\,\mathrm{Re}\,\langle \psi_{\mathrm{inc}}, \phi \rangle \tag{15}$$

where the inner product is defined by $\langle a, b\rangle = \int_A a^\dagger b \, \mathrm{d}A$. For the most general bounds in the main text, Eq. (4), we assume only that the fields are currents are related by some linear operator $\mathcal{L}$,

$$\mathcal{L}\,\phi = \psi, \tag{16}$$

where we have generalized the $\mathcal{L}$ operator from the main text, to include magnetic currents.

The simplest bound to derive is the one for scattered power. We substitute the constitutive equation, Eq. (16), in the equations for absorption and extinction, and write the scattered power as the difference between extinction and absorption:

$$P_{\mathrm{scat}} = \frac{1}{2}\left[\frac{1}{2}\left\langle \psi_{\mathrm{inc}}, \phi\right\rangle + \frac{1}{2}\left\langle \phi, \psi_{\mathrm{inc}}\right\rangle - \left\langle \phi, (\mathrm{Re}\,\mathcal{L})\,\phi\right\rangle\right] \tag{17}$$

Note that by passivity $\mathrm{Re}\,\mathcal{L}$ is positive-definite (for a scalar isotropic conductivity, $\mathrm{Re}\,\mathcal{L} > 0$ is equivalent to $\mathrm{Re}\,\sigma > 0$). Thus the negative term in Eq. (17) is a positive-definite quadratic function of the currents ϕ, whereas the first two positive terms are only *linear* in ϕ. Thus P_{scat} is inherently bounded by constraints imposed by the optical-theorem form of the extinction. We can find the extremum by setting the variational derivative $\delta/\delta\phi^*$ equal to zero:

$$\frac{\delta P_{\mathrm{scat}}}{\delta \phi^*} = \frac{1}{4}\psi_{\mathrm{inc}} - \frac{1}{2}\,(\mathrm{Re}\,\mathcal{L})\,\phi = 0 \tag{18}$$

which implies that the optimal currents are given by

$$\phi = \frac{1}{2}\,(\mathrm{Re}\,\mathcal{L})^{-1}\,\psi_{\mathrm{inc}} \tag{19}$$

For these optimal currents, the scattered power is given by direct substitution of Eq. (19)

into Eq. (17), yielding

$$P_{\text{scat}} \leq \frac{1}{8} \left\langle \psi_{\text{inc}}, (\text{Re}\, \mathcal{L})^{-1} \psi_{\text{inc}} \right\rangle . \tag{20}$$

Equation (20) is the magnetic-current generalization of the scattered-power component of Eq. (4) in the main text. By similar variational derivatives, with a Lagrangian-multiplier approach to the constraint $P_{\text{abs}} < P_{\text{ext}}$, the bounds on P_{abs} and P_{ext} follow:

$$P_{\text{abs,ext}} \leq \frac{1}{2} \left\langle \psi_{\text{inc}}, (\text{Re}\, \mathcal{L})^{-1} \psi_{\text{inc}} \right\rangle , \tag{21}$$

with the only difference from the scattered-power bound being the extra factor of four (the β term in the main text), which arises because maximization of absorption or extinction can fully "saturate" the constraint, i.e. $P_{\text{abs}} = P_{\text{ext}}$. Similar saturation would yield no scattered power, and thus the scattered-power optimum occurs for $P_{\text{abs}} = P_{\text{scat}} = \frac{1}{2} P_{\text{ext}}$, at half the current level and thus one-fourth of the power level.

The next equation from the main text that we want to show the key steps for is Eq. (7), the bound for the LDOS. In this case, we can consider a spatially local conductivity for the $\mathcal{L}$ operator, i.e., $\mathcal{L} = \boldsymbol{\sigma}^{-1}$. We henceforth do not consider magnetic currents, though the generalization is straightfoward. The bound for the LDOS takes exactly the same form as Eqs. (20,21), for absorption, scattering, and extinction, but with a different prefactor to account for the free-space LDOS, ρ_0:

$$\begin{aligned} \frac{\rho_\alpha}{\rho_0} &\leq \beta_\alpha \frac{1}{\varepsilon_0 \omega} \frac{2\pi}{k^3} \sum_j \left\langle \mathbf{E}_{\text{inc},j}, \left(\text{Re}\, \boldsymbol{\sigma}^{-1}\right)^{-1} \mathbf{E}_{\text{inc},j} \right\rangle \\ &= \beta_\alpha \frac{1}{\varepsilon_0 \omega} \frac{2\pi}{k^3} \left\| \boldsymbol{\sigma}^\dagger \left(\text{Re}\, \boldsymbol{\sigma}\right)^{-1} \boldsymbol{\sigma} \right\|_2 \sum_j \int_A |\mathbf{E}_{\text{inc},j}|^2 \, \text{d}A \end{aligned} \tag{22}$$

where j denotes the (random) orientation of the dipolar emitter, α denotes either the total, radiative, or nonradiatve LDOS, and β_α is 1 for the total or nonradiative LDOS and 1/4

for the radiative LDOS (and we have dropped an additive +1 factor for the radiative LDOS that is negligible in the near field). The surface A of the 2D material can take any shape; because the integrand in Eq. (22) is positive, we can find the planar surface passing through the point on A that is closest to the emitter. Denoting this half space Γ, we know that

$$\int_A |\mathbf{E}_{\text{inc}}|^2 \, \mathrm{d}A \leq \int_\Gamma |\mathbf{E}_{\text{inc}}|^2 \, \mathrm{d}A \tag{23}$$

where the latter expression can be analytically evaluated due to its symmetry. [As discussed in the main text, other bounding surfaces (such as the closest spherical shell) can be used, instead of a half space, with the resulting difference only being different numerical prefactors. To determine the integral, we can use the fact that the sum of the squared electric field over all source-dipole orientations is given by the Frobenius norm of the dyadic electric-field Green's function:

$$\sum_j |\mathbf{E}_{\text{inc},j}|^2 = \|\boldsymbol{G}_0\|_F^2 = \frac{k^6}{8\pi^2}\left[\frac{3}{(kr)^6} + \frac{1}{(kr)^4} + \frac{1}{(kr)^2}\right] \tag{24}$$

which has contributions from $1/r^6$, $1/r^4$, and $1/r^2$ terms. The $1/r^2$ term represents a far field radiative contribution, which is dominated in the near field by higher-order terms. The integrals of $1/r^6$ and $1/r^4$ over the plane Γ are

$$\int_\Gamma \frac{1}{r^6} \, \mathrm{d}A = \frac{\pi}{2d^4} \tag{25a}$$

$$\int_\Gamma \frac{1}{r^4} \, \mathrm{d}A = \frac{\pi}{d^2} \tag{25b}$$

where d is the separation of the emitter from the plane Γ. Thus the integral over the Frobenius norm of the Green's function, excluding the far-field term, is

$$\int_\Gamma \|\boldsymbol{G}_0\|_F^2 \, \mathrm{d}A = \frac{k^4}{8\pi}\left[\frac{3}{2(kd)^4} + \frac{1}{(kd)^2}\right] \tag{26}$$

Inserting this value into the bound of Eq. (22) yields:

$$\frac{\rho_\alpha}{\rho_0} \leq \beta_\alpha \left\| \boldsymbol{\sigma}^\dagger \left(\operatorname{Re} \boldsymbol{\sigma}\right)^{-1} \boldsymbol{\sigma} \right\|_2 \left[\frac{3}{8(kd)^4} + \frac{1}{4(kd)^2} \right], \tag{27}$$

which is the LDOS bound of Eq. (7) in the main text, including the second-order term.

The final expression whose mathematical form we want to derive is the RHT bound of Eq. (8) in the main text. As explained in the main text, and derived in Ref. 6, a bound on RHT can be developed by consideration of two scattering problems connected through (generalized) reciprocity. For two surfaces with conductivities $\boldsymbol{\sigma}_1$ and $\boldsymbol{\sigma}_2$, the bound is of the form

$$\begin{aligned} \Phi(\omega) \leq & \frac{2}{\pi \varepsilon_0^2 \omega^2} \left\| \left(\operatorname{Re} \boldsymbol{\sigma}_1^{-1}\right)^{-1} \right\|_2 \left\| \left(\operatorname{Re} \boldsymbol{\sigma}_2^{-1}\right)^{-1} \right\|_2 \\ & \times \int_{A_1} \int_{A_2} \left\| \boldsymbol{G}_0(\mathbf{x}_1, \mathbf{x}_2) \right\|_F^2 \, \mathrm{d}^2\mathbf{x}_1 \mathrm{d}^2\mathbf{x}_2. \end{aligned} \tag{28}$$

To complete the integral over the two 2D surfaces, we use the same "bounding plane" approach as for the LDOS. Now we need a double integral over Γ_1 and Γ_2, where Γ_1 and Γ_2 are the bounding planes for A_1 and A_2:

$$\int_{\Gamma_1} \int_{\Gamma_2} \frac{1}{r^6} = A \int_{\Gamma_2} \frac{1}{r^6} = \frac{\pi A}{2d^4} \tag{29}$$

$$\int_{\Gamma_1} \int_{\Gamma_2} \frac{1}{r^4} = A \int_{\Gamma_2} \frac{1}{r^4} = \frac{\pi A}{d^2} \tag{30}$$

where A is the (infinite) area of the Γ_1 and Γ_2 surfaces, which could be pulled out of the integrals by symmetry. Inserting the integrals into the RHT bound expression in Eq. (28) yields:

$$\begin{aligned} \Phi(\omega) \leq & \frac{k^2 A}{4\pi^2} Z_0^2 \left\| \left(\operatorname{Re} \boldsymbol{\sigma}_1^{-1}\right)^{-1} \right\|_2 \left\| \left(\operatorname{Re} \boldsymbol{\sigma}_2^{-1}\right)^{-1} \right\|_2 \\ & \times \left[\frac{3}{2(kd)^4} + \frac{1}{4(kd)^2} \right]. \end{aligned} \tag{31}$$

Recognizing that $k^2A/4\pi^2$ is precisely the blackbody flux rate,[7] Φ_{BB}, we can write

$$\begin{aligned}\frac{\Phi(\omega)}{\Phi_{\mathrm{BB}}(\omega)} \leq & Z_0^2 \left\| \left(\mathrm{Re}\, \boldsymbol{\sigma}_1^{-1} \right)^{-1} \right\|_2 \left\| \left(\mathrm{Re}\, \boldsymbol{\sigma}_2^{-1} \right)^{-1} \right\|_2 \\ & \times \left[\frac{3}{2(kd)^4} + \frac{1}{4(kd)^2} \right],\end{aligned} \tag{32}$$

which is precisely the RHT bound of Eq. (8) in the main text, except that here we allow for two different materials in the interaction, and we include the second-order distance term, proportional to $1/d^2$.

5 Bounds in the presence of hydrodynamic nonlocality

In the main text, we showed that in a general Maxwell-equation framework, hydrodynamic nonlocality *cannot* increase maximum optical response, as any such nonlocal response is subject to the local-response bound. Here we show that under the additional assumption of *quasistatic* response, which will almost always apply at the length scales for which nonlocal effects are non-negligible, the nonlocality necessarily *reduces* the maximum achievable optical response in a given 2D material. In accord with typical hydrodynamic models,[8] we will work only with electric surface currents $\mathbf{K}$, driven by electric fields $\mathbf{E}$, related by Eq. (10) of the main text, repeated here in compact notation:

$$-A\nabla\nabla\cdot\mathbf{K} + B\mathbf{K} = \mathbf{E}, \tag{33}$$

where

$$A = \frac{i}{\varepsilon_0\omega\omega_{\mathrm{p}}^2}\left(\beta^2 + D\left(\gamma - i\omega\right)\right), \tag{34a}$$

$$B = \sigma_{\mathrm{loc}}^{-1}, \tag{34b}$$

σ_{loc} is the local surface conductivity, and $\beta^2 = (3/5)v_F^2$ (for Fermi velocity v_F) for both parabolic 2D materials as well as graphene. Note that one can define the plasma frequency ω_p using $\hbar k_{\text{F}}/v_{\text{F}}$ as the effective mass, yielding $\omega_p^2 = e^2 E_{\text{F}}/(\pi\varepsilon_0\hbar^2)$. In the presence of a hydrodynamic nonlocality, it is straightforward to write the absorbed power in terms of the currents $\mathbf{K}$:

$$\begin{aligned} P_{\text{abs}} &= \frac{1}{2}\,\text{Re}\int_A \mathbf{K}^* \cdot \mathbf{E} \\ &= \frac{1}{2}\,\text{Re}\int_A -A\mathbf{K}^* \cdot \nabla\nabla \cdot \mathbf{K} + B\mathbf{K}^* \cdot \mathbf{K} \\ &= \frac{1}{2}\int_A a\,(\nabla \cdot \mathbf{K}^*)\,(\nabla \cdot \mathbf{K}) + b\mathbf{K}^* \cdot \mathbf{K}, \end{aligned} \tag{35}$$

where the second line follows from integration by parts and the no-spillout condition ($\hat{\mathbf{n}} \cdot \mathbf{K} = 0$), and a and b are the real parts of A and B, respectively,

$$a = \text{Re}(A) = \frac{D}{\varepsilon_0 \omega_{\text{p}}^2}, \tag{36a}$$

$$b = \text{Re}(B) = \text{Re}\left(\sigma_{\text{loc}}^{-1}\right), \tag{36b}$$

which are positive by the sign convention chosen in Eq. (33). The key insight to take away from Eq. (35) is that it is quadratic in $\mathbf{K}$ *and* $\nabla \cdot \mathbf{K}$. Thus for nonlocal models, restrictions on the *divergence* of the currents represent an additional constraint on maximal optical response. To have a non-trivial restriction on $\nabla \cdot \mathbf{K}$, there should also be a term in the extinction that is linear in $\nabla \cdot \mathbf{K}$. This is where the quasistatic approximation is useful. Quasisatic electromagnetism dictates that the incident field is the (negative) gradient of some potential ϕ_{inc}: $\mathbf{E}_{\text{inc}} = -\nabla\phi_{\text{inc}}$. Then, using integration by parts and the no-spillout

condition once more, we can write the extinction in either of two equivalent ways:

$$P_{\text{ext}}^{(1)} = \frac{1}{2}\,\text{Re}\int_A \mathbf{E}_{\text{inc}}^* \cdot \mathbf{K}, \tag{37}$$

$$P_{\text{ext}}^{(2)} = \frac{1}{2}\,\text{Re}\int_A \phi_{\text{inc}}^* \nabla \cdot \mathbf{K}. \tag{38}$$

The first equation, Eq. (37), offers a constraint on the magnitude of $\mathbf{K}$, while the second equation, Eq. (38), offers a constraint on the magnitude of $\nabla \cdot \mathbf{K}$. Thus if we wish to maximize extinction, for example, it is subject to two constraints, $P_{\text{abs}} < P_{\text{ext}}^{(1)}$ and $P_{\text{abs}} < P_{\text{ext}}^{(2)}$, and we should maximize the *minimum* of $P_{\text{ext}}^{(1)}$ and $P_{\text{ext}}^{(2)}$ (which are not necessarily equivalent since we do not impose the additional nonconvex constraint of satisfying quasistatic electromagnetism). Thus the maximal-extinction problem can be written as a "maximin" (negative of a minimax) convex problem

$$\begin{aligned} \max_{\mathbf{K},\nabla\cdot\mathbf{K}} \min_{i\in\{1,2\}} \quad & P_{\text{ext}}^{(i)} \\ \text{such that} \quad & P_{\text{abs}} \le P_{\text{ext}}^{(i)}. \end{aligned} \tag{39}$$

Although Eq. (39) is nonsmooth (because of the absolute value), a standard transformation[9] yields an equivalent smooth optimization problem

$$\begin{aligned} \max_{\mathbf{K},\nabla\cdot\mathbf{K},x} \quad & x \\ \text{such that} \quad & x \le P_{\text{ext}}^{(i)} \\ & P_{\text{abs}} \le P_{\text{ext}}^{(i)}, \end{aligned} \tag{40}$$

where $i \in \{1,2\}$ and the constraints are all convex. At the extremum $P_{\text{ext}}^{(1)} = P_{\text{ext}}^{(2)}$, and standard optimization techniques (e.g., Lagrange multipliers) yield this optimal value:

$$P_{\text{ext}} \le \frac{1}{2}\left[\frac{\text{Re}(\sigma_{\text{loc}}^{-1})}{\int_A |\mathbf{E}_{\text{inc}}|^2} + \frac{D/(\varepsilon_0\omega_{\text{p}}^2)}{\int_A |\phi_{\text{inc}}|^2}\right]^{-1}. \tag{41}$$

The bound on the right-hand side of Eq. (41) is a rate competition between the local-conductivity bound in the first term and a diffusion-constant-based bound in the second term that only arises from the hydrodynamic nonlocality. We can simplify the bound in the case of a plane wave.

Within the quasistatic approximation, an incident plane wave is represented by a constant vector field across/over the surface of the 2D material; for a polarization along $\hat{\mathbf{z}}$, i.e. for $\mathbf{E}_{\text{inc}} = E_0\hat{\mathbf{z}}$, the associated potential is $\phi_{\text{inc}} = -E_0 z$. If the "radius" of the scatterer (more precisely, its smallest bound sphere in the polarization direction) is given by r, we can simplify the integral of $|\phi_{\text{inc}}|^2$ via the inequality

$$\int_A |\phi_{\text{inc}}|^2 = |E_0|^2 \int_A z^2 = |E_0|^2 \left\langle z^2 \right\rangle A \leq |E_0|^2 r^2 A, \tag{42}$$

where $\langle\cdot\rangle$ denotes an average over the area of the scatterer. In terms of the cross-section, $\sigma_{\text{ext}} = P_{\text{ext}}/(|E_0|^2/2Z_0)$, the expression of Eq. (41) is bounded above by

$$\frac{\sigma_{\text{ext}}}{A} \leq \left[\left(Z_0 \frac{|\sigma_{\text{loc}}|^2}{\text{Re}\,\sigma_{\text{loc}}} \right)^{-1} + \left(\frac{r^2}{\ell_D^2} \right)^{-1} \right]^{-1}, \tag{43}$$

where $\ell_D = \sqrt{\frac{cD}{\omega_{\text{p}}^2}}$ is a normalized diffusivity that we can interpret as a plasmonic "diffusion" length. Equation (43) has an appealing, intuitive interpretation: the cross-section of a scatterer is bounded above by a combination of the local-conductivity bound and a nonlocal contribution proportional to the square of the ratio of the size of the scatterer to the "diffusion" length. Thus as the size of the particle approaches ℓ_D, and goes below it, there is a significant reduction in the maximal optical response.

Because the local density of states (LDOS) is proportional to Eq. (37), but with the replacement $\mathbf{E}_{\text{inc}}^* \to \mathbf{E}_{\text{inc}}$ (Ref. 10), the equivalent LDOS bound is exactly Eq. (41), with additional numerical prefactors and the caveat that $\mathbf{E}_{\text{inc}}$ is now rapidly decaying in space. The $1/r^3$ decay of the incident field is responsible for the $1/d^4$ distance dependence of the

local-conductivity LDOS bound, Eq. (7), in the main text. But the incident-field potential, ϕ_{inc}, decays less rapidly, with scaling $\sim 1/r^2$. Thus $\int_A |\phi_{\text{inc}}|^2 \sim 1/d^2$, a dramatic reduction from the $1/d^4$ scaling for a local conductivity. The crossover from the $1/d^4$ term being dominant in the bound to the $1/d^2$ term being dominant occurs when the separation distance d is of the same order of magnitude as the diffusion length ℓ_D. Exploration of the $1/d^2$ scaling in various relevant materials and geometries would be interesting future work.

6 LDOS above a planar conducting sheet

In this section we analytically derive the LDOS above a planar conducting sheet. We show that the envelope of the peak LDOS has $1/d^3$ scaling when dominated by a single resonance, whereas it has a $1/d^4$ scaling, and comes within a factor of two of the LDOS bounds of Eq. (7) in the main text, when it arises from a "lossy-background" contribution. The LDOS above any structure with translational and rotational symmetry is given by

$$\rho(\omega) = \int \rho(\omega, k_p)\, \mathrm{d}k_p \tag{44}$$

where k_p is the magnitude of the surface-parallel component of the wavevector. In the near field ($k_p \gg k_0$), for p-polarized waves (e.g., surface plasmons), $\rho(\omega, k_p)$ is given by

$$\rho(\omega, k_p) = \frac{k_0}{2\pi^2 c} \frac{k_p^2}{k_0^2} e^{-2k_p z} \operatorname{Im} r_p \tag{45}$$

where r_p is the p-polarized (TM) reflection coefficient. For a 2D material with surface conductivity σ, r_p is given by

$$r_p \approx \frac{i\sigma k_p}{2\varepsilon_0 \omega + i\sigma k_p} \tag{46}$$

$$= \frac{k_p}{k_p - \xi} \tag{47}$$

where $\xi = i2\varepsilon_0\omega/\sigma$. Thus the imaginary part of the reflection coefficient is

$$\operatorname{Im} r_p = \frac{k_p \xi''}{(k_p - \xi)' + (\xi'')^2}, \tag{48}$$

where the single and double apostrophes indicate real and imaginary parts, respectively. The variable $\xi(\omega)$ encodes the material conductivity. For single-resonance-dominant response, the wavevector integral of Eq. (45) will be dominated by a narrow peak in the imaginary part of the reflection coefficient, i.e. Eq. (48), where $k_p \approx \xi'$. Conversely, for a highly lossy background, for which $\operatorname{Re}\sigma \gg |\operatorname{Im}\sigma|$ and thus $\operatorname{Im}\xi \gg |\operatorname{Re}\xi|$, the contribution of $\operatorname{Im} r_p$ to the integrand in Eq. (28) will be roughly constant. We treat the two cases separately.

6.1 Pole contribution to the LDOS

As discussed above, the imaginary part of the reflection coefficient will be sharply peaked around $k_p \approx \operatorname{Re}\xi(\omega)$ in the case of a single resonance dominating the response. Then the peak value of $\operatorname{Im} r_p$, as a function of wavevector, will be

$$\max \operatorname{Im} r_p \approx \frac{k_p}{\xi''} \tag{49}$$

and the width of the peak will be $\Delta k_p \approx 2\xi''$. If we denote k_{p0} as the peak wavevector at which $\operatorname{Im} r_p$ takes its maximum value, and assume a Lorentzian lineshape for $\operatorname{Im} r_p$, then we can approximate the k_p-dependent terms in the integral of Eq. (45) by

$$\begin{aligned}
\int k_p^2 e^{-2k_p z} \operatorname{Im}(r_p)\, \mathrm{d}k_p &\approx k_{p0}^2 e^{-2k_{p0} z} \int \operatorname{Im}(r_p)\, \mathrm{d}k_p \\
&\approx k_{p0}^2 e^{-2k_{p0} z} \frac{\pi}{2} \operatorname{Im}\left[r_p(k_{p0})\right] \Delta k_p \\
&= \pi k_{p0}^3 e^{-2k_{p0} z}
\end{aligned} \tag{50}$$

Thus we can write the full LDOS, $\rho(\omega)$, as

$$\rho(\omega) = \rho_0(\omega)\frac{k_{p0}^3}{k_0^3}e^{-2k_{p0}z}, \tag{51}$$

where $\rho_0(\omega)$ is the electric-only free-space LDOS, $\rho_0 = k_0^2/2\pi^2 c$. We note that the optimal frequency, and thus the optimal k_{p0}, changes as a function of z, with the optimal k_{p0} given by $k_{p0} = 3/2z$. Replacing the height z with the separation distance d, we can write

$$\begin{aligned}\max_{\omega}\frac{\rho(\omega)}{\rho_0(\omega)} &\approx \pi\left(\frac{3}{2e}\right)^3\frac{1}{(k_0 d)^3}\\ &\approx \frac{1}{2(k_0 d)^3}.\end{aligned} \tag{52}$$

The expression given by Eq. (52) quantitatively predicts the short-distance and low-frequency behavior of the LDOS in Fig. 3 of the main text.

6.2 Lossy-background contribution to the LDOS

The lossy-background contribution to the LDOS exhibits a different mathematical structure. Instead of $\operatorname{Im} r_p$ being sharply peak around a single resonance, $\operatorname{Im}\xi \gg |\operatorname{Re}\xi|$, and the imaginary part of the reflectivity is nearly constant over wavevector:

$$\operatorname{Im} r_p \approx \frac{k_p}{\xi''} \tag{53}$$

for all k_p (that are not so large as to be inaccessible at a finite separation distance). Thus $\operatorname{Im} r_p$ can be taken out of the integral for ρ, Eq. (45), which is then given by

$$\begin{aligned}\int k_p^2 e^{-2k_p z}\operatorname{Im} r_p \,\mathrm{d}k_p &\approx \frac{1}{\xi''}\int k_p^3 e^{-2k_p z}\,\mathrm{d}k_p\\ &\approx \frac{1}{\xi''}\frac{3}{8z^4},\end{aligned} \tag{54}$$

where we have kept ony the lowest-order term in $1/z$. Writing out $\xi'' = 2\varepsilon_0\omega/\operatorname{Re}\sigma$, straightforward algebra yields:

$$\frac{\rho(\omega)}{\rho_0(\omega)} \approx \frac{3}{16}\,(Z_0 \operatorname{Re}\sigma)\,\frac{1}{(k_0 d)^4} \tag{55}$$

for emitter–material separation distance d. We see that in the limit $\operatorname{Re}\sigma \gg |\operatorname{Im}\sigma|$, which is a prerequisite for the lossy-background contribution to dominate, Eq. (55) is exactly a factor of 2 smaller than the general LDOS bound that appears in Eq. (7) of the main text. The factor of 2 stems from the factor of 2 in the denominator of Eq. (46), which itself arises from the equal interactions of a 2D material with the exterior regions on either side of its surface. Equation (55) quantitatively predicts the LDOS in the moderate-separation and large-energy regimes of Fig. 3 of the main text.

References

(1) F. Javier Garcia de Abajo and Alejandro Manjavacas, "Plasmonics in Atomically Thin Materials," Faraday Discuss. **178**, 87–107 (2015).

(2) Thomas Christensen, *From Classical to Quantum Plasmonics in Three and Two Dimensions*, Ph.D. thesis, Technical University of Denmark (2017).

(3) Feng Wang and Y. Ron Shen, "General Properties of Local Plasmons in Metal Nanostructures," Phys. Rev. Lett. **97**, 206806 (2006).

(4) Aaswath Raman, Wonseok Shin, and Shanhui Fan, "Upper Bound on the Modal Material Loss Rate in Plasmonic and Metamaterial Systems," Phys. Rev. Lett. **110**, 183901 (2013).

(5) William M. Haynes, *CRC Handbook of Chemistry and Physics* (CRC press, 2013).

(6) Owen D. Miller, Steven G. Johnson, and Alejandro W Rodriguez, "Shape-independent limits to near-field radiative heat transfer," Phys. Rev. Lett. **115**, 204302 (2015).

(7) Karl Joulain, Jean-Philippe Mulet, François Marquier, Rémi Carminati, and Jean-Jacques Greffet, "Surface electromagnetic waves thermally excited: Radiative heat transfer, coherence properties and Casimir forces revisited in the near field," Surf. Sci. Rep. **57**, 59–112 (2005).

(8) N. A. Mortensen, S. Raza, M. Wubs, T. Søndergaard, and S. I. Bozhevolnyi, "A generalized non-local optical response theory for plasmonic nanostructures," Nat. Commun. **5**, 3809 (2014).

(9) Jorge Nocedal and Stephen J Wright, *Numerical Optimization*, 2nd ed. (Springer, New York, NY, 2006).

(10) Owen D. Miller, Athanasios G. Polimeridis, M. T. Homer Reid, Chia Wei Hsu, Brendan G. DeLacy, John D. Joannopoulos, Marin Soljačić, and Steven G. Johnson, "Fundamental limits to optical response in absorptive systems," Opt. Express **24**, 3329–64 (2016).